CHEMISTRY OF MATERIALS
Article

Chem. Mater. **2010,** *22,* 2597–2607 2597
DOI:10.1021/cm903664g

Synthesis, Characterization, and Surface Initiated Polymerization of Carbazole Functionalized Isocyanides

Erik Schwartz,[†,#] Eunhee Lim,[‡,#,▽] Chandrakala M. Gowda,[§] Andrea Liscio,[⊥] Oliver Fenwick,[∥] Guoli Tu,[‡] Vincenzo Palermo,[⊥] Rene de Gelder,[†] Jeroen J. L. M. Cornelissen,*[,†,◆] Ernst R. H. Van Eck,[§] Arno P. M. Kentgens,[§] Franco Cacialli,*[,∥] Roeland J. M. Nolte,[†] Paolo Samorì,*[,⊥,○] Wilhelm T. S. Huck,*[,‡] and Alan E. Rowan*[,†]

[†]*Radboud University Nijmegen, Institute for Molecules and Materials, Department of Organic Chemistry, Heyendaalseweg 135, 6525 AJ Nijmegen, The Netherlands,* [‡]*Melville Laboratory for Polymer Synthesis, Department of Chemistry, University of Cambridge, Lensfield Road, Cambridge CB2 1EW, United Kingdom,* [§]*Radboud University Nijmegen, Institute for Molecules and Materials, Department of Physical Chemistry/Solid State NMR, Heyendaalseweg 135, 6525 AJ Nijmegen, The Netherlands,* [⊥]*Istituto per la Sintesi Organica e la Fotoreattività, Consiglio Nazionale delle Ricerche Via Gobetti 101, I-40129 Bologna, Italy,* [∥]*Department of Physics and Astronomy and London Centre for Nanotechnology, University College London, Gower Street London, United Kingdom, WC1E 6BT, and* [○]*Nanochemistry Laboratory, ISIS, Université de Strasbourg and CNRS (UMR 7006) 8 allée Gaspard Monge, F-67000 Strasbourg, France.* [#] *These authors contributed equally to this work.* [▽] *Present address: Korea Institute of Industrial Technology (KITECH), 35-3, Hongcheonri, Ipjangmyeon, Cheonansi, Chungnam 330-825, Republic of Korea.* [◆] *Present address: Laboratory for Biomolecular Nanotechnology, MESA+ Institute, University of Twente, Enschede, The Netherlands.*

Received December 4, 2009. Revised Manuscript Received January 26, 2010

We describe the design and synthesis of carbazole functionalized isocyanides and the detailed investigation of their properties. Characterization by solid state NMR, CD, and IR spectroscopic techniques reveals that the polymer has a well-defined helical architecture. Surface-initiated polymerization of the isocyanide monomers onto various surfaces was carried out to give polymer brushes up to 150 nm thick. Insights into the electronic properties of the materials were obtained by Kelvin probe force microscopy (KPFM) and electroabsorption studies.

1. Introduction

Carbazole based materials are well-known for their favorable hole-transport and electroluminescent properties and have therefore been investigated extensively.[1,2] In general, two methods are utilized for the preparation of carbazole containing polymers. The first is to use a carbazole derivative that can, for example, undergo metal-catalyzed polycondensation reactions such as Suzuki[3] or Stille[4] couplings, to obtain main-chain carbazole random (co)polymers. The second approach is to use a polymer scaffold to which carbazole moieties can be attached, such as polyacetylenes,[5,6] poly(*N*-vinylcarbazole),[7] polymethacrylates,[8] poly(*p*-phenylenevinylene),[9] and poly-((amino)-amide)s.[10] The unique properties of the polymers allow for

*Corresponding authors. E-mail: j.j.l.m.cornelissen@tnw.utwente.nl (J.J.L.M.C.); f.cacialli@ucl.ac.uk (F.C.); samori@isis-ulp.org (P.S.); wtsh2@cam.ac.uk (W.T.S.H.); a.rowan@science.ru.nl (A.E.R.).

(1) Grazulevicius, J. V.; Strohriegl, P.; Pielichowski, J.; Pielichowski, K. *Prog. Polym. Sci.* **2003**, *28*(9), 1297–1353.
(2) Blouin, N.; Leclerc, M. *Acc. Chem. Res.* **2008**, *41*(9), 1110–1119.
(3) Schlüter, A. D. *J. Polym. Sci. Part A: Polym. Chem.* **2001**, *39*(10), 1533–1556.
(4) Bao, Z.; Chan, W. K.; Yu, L. *J. Am. Chem. Soc.* **2002**, *117*(50), 12426–12435.
(5) Qu, J. Q.; Suzuki, Y.; Shiotsuki, M.; Sanda, F.; Masuda, T. *Polymer* **2007**, *48*(16), 4628–4636.
(6) (a) Sanda, F.; Kawaguchi, T.; Masuda, T.; Kobayashi, N. *Macromolecules* **2003**, *36*(7), 2224–2229. (b) Sanda, F.; Nakai, T.; Kobayashi, N.; Masuda, T. *Macromolecules* **2004**, *37*(8), 2703–2708. (c) Takihana, Y.; Shiotsuki, M.; Sanda, F.; Masuda, T. *Macromolecules* **2004**, *37*(20), 7578–7583. (d) Tamura, K.; Fujii, T.; Shiotsuki, M.; Sanda, F.; Masuda, T. *Polymer* **2008**, *49*(21), 4494–4501. (e) Fulghum, T.; Karim, S. M. A.; Baba, A.; Taranekar, P.; Nakai, T.; Masuda, T.; Advincula, R. C. *Macromolecules* **2006**, *39*(4), 1467–1473.
(7) (a) Gong, X.; Wang, S.; Moses, D.; Bazan, G. C.; Heeger, A. J. *Adv. Mater.* **2005**, *17*(17), 2053–2058. (b) Kawamura, Y.; Yanagida, S.; Forrest, S. R. *J. Appl. Phys.* **2002**, *92*(1), 87–93.
(8) (a) Angiolini, L.; Benelli, T.; Giorgini, L.; Mauriello, F.; Salatelli, E. *Macromol. Chem. Phys.* **2006**, *207*(20), 1805–1813. (b) Bogdal, D.; Yashchuk, V.; Pielichowski, J.; Ogul'Chansky, T.; Warzala, M.; Kudrya, V. *J. Appl. Polym. Sci.* **2002**, *84*(9), 1650–1656. (c) Engels, C.; Van Steenwinckel, D.; Hendrickx, E.; Schaerlaekens, M.; Persoons, A.; Samyn, C. *J. Mater. Chem.* **2002**, *12*(4), 951–957. (d) Huang, C. Y.; Jiang, G. Q.; Advincula, R. *Macromolecules* **2008**, *41*(13), 4661–4670.
(9) (a) Kim, K.; Hong, Y. R.; Lee, S. W.; Jin, J. I.; Park, Y.; Sohn, B. H.; Kim, W. H.; Park, J. K. *J. Mater. Chem.* **2001**, *11*(12), 3023–3030. (b) Liang, F.; Kurata, T.; Nishide, H.; Kido, J. *J. Polym. Sci., Part A: Polym. Chem.* **2005**, *43*(23), 5765–5773. (c) Vellis, P. D.; Mikroyannidis, J. A.; Cho, M. J.; Choi, D. H. *J. Polym. Sci., Part A: Polym. Chem.* **2008**, *46*(16), 5592–5603. (d) Ravindranath, R.; Ajikumar, P. K.; Bahulayan, S.; Hanafiah, N. B. M.; Baba, A.; Advincula, R. C.; Knoll, W.; Valiyaveettil, S. *J. Phys. Chem. B* **2007**, *111*(23), 6336–6343.
(10) (a) Liou, G. S.; Chen, H. W.; Yen, H. J. *J. Polym. Sci., Part A: Polym. Chem.* **2006**, *44*(13), 4108–4121. (b) Liou, G. S.; Hsiao, S. H.; Huang, N. K.; Yang, Y. L. *Macromolecules* **2006**, *39*(16), 5337–5346.
(11) Kippelen, B.; Golemme, A.; Hendrickx, E.; Wang, J. F.; Marder, S. R.; Peyghambarian, N. Photorefractive Polymers and Polymer-Dispersed Liquid Crystals. In *Field Responsive Polymers: Electroresponsive, Photoresponsive, and Responsive Polymers in Chemistry and Biology*; Khan, I. M., Harrison, J. S., Eds.; American Chemical Society: Washington, DC, 1999; Vol. *726*, p 204.

Published on Web 03/15/2010

photonic applications such as electroluminescent, photorefractive, or xerographic materials.[1,11] More recently, poly(2,7-carbazole)s have also been applied in organic light-emitting diodes (OLEDs), organic field-effect transistors (OFETs), and photovoltaic devices.[2]

Polyisocyanides are unique polymers that exhibit a well-defined structure[12] and high stiffness[13] due to their helical backbone. The introduction of chiral peptidic fragments induces the side arms to adopt a β-sheet like arrangement due to the formation of a hydrogen bonding network between the amide groups.[14] They therefore form attractive scaffolds for the arrangement of electronically and optically interesting molecules, as was shown by us and others over the recent years.[15] As carbazoles are easily functionalized at the nitrogen atom and have favorable thermal, electrical, and photophysical properties, we were interested to incorporate carbazole groups into polyisocyanides. Here, we present our studies on carbazole functionalized polyisocyanopeptides and their detailed characterization by IR and solid state NMR spectroscopies. In addition, polymer brushes provide a potential route to control the orientation of polymers in optoelectronic devices.[16] Recently, we reported the growth of helical polyisocyanopeptide (poly-L-isocyanoalanyl-L-alanine methyl ester, LL-PIAA) brushes.[17] The morphology of these brushes showed unusual featherlike structures, as visualized by atomic force microscopy (AFM). We also confirmed that the brushes retained their helical conformation (circular dichroism spectroscopy, CD) and hydrogen-bonding network (infrared spectroscopy, IR). In this paper we expand this work, by using a functionalized polyisocyanide (i.e., a carbazole containing polymer) that allows us to gain more information about the (electronic) properties of the polymer. By using a surface covered with Ni catalysts, polymer brushes up to 150 nm in length could be prepared. These polymer brushes were characterized by CD and IR spectroscopy and by AFM. Kelvin Probe measurements performed on both the macroscopic (KP) and submicroscopic (KPFM) scale offered a more detailed investigation into the electronic properties of the resultant polymer films.

2. Experimental Section

General. All solvents were distilled prior to use. All other chemicals were commercials products and used as received. Column chromatography was performed using silica gel (40−60 μm) purchased from Merck. TLC analyses were carried out on silica 60 F_{254} coated glass from Merck, and the compounds were visualized using ninhydrine or $Ni(ClO_4)_2 \cdot 6H_2O$ in EtOH. ^{1}H NMR and ^{13}C NMR spectra were recorded on a Bruker AC-300 MHz instrument operating at 300 and 75 MHz, respectively, unless otherwise stated. FT-infrared spectra were recorded on a ThermoMattson IR300 spectrometer equipped with a Harrick ATR unit; compounds were measured as solid. The solution infrared spectra were measured on a Bruker Tensor 27 in a fluid cell of KBr. Mass spectrometry measurements were performed on a JEOL Accutof instrument (ESI). Elemental analyses were obtained using a Carlo Erba 1180 instrument. Optical rotations were measured on a Perkin-Elmer 241 Polarimeter at room temperature and are reported in 10^{-1} deg cm^2 g^{-1}. UV−vis spectra were recorded on a Varian Cary 50 spectrometer, and fluorescence spectra, on a Perkin-Elmer Luminescence spectrometer LS50B. Differential scanning calorimetry (DSC) was carried out on a Perkin-Elmer DSC-7. Circular dichroism (CD) spectra of the polymer brushes were recorded on an Applied Photophysics Chirascan circular dichroism spectrophotometer at 25 °C. UV−vis absorption spectra of the polymer brushes were obtained with a Varian 4000 UV−vis spectrophotometer. The isocyanide monomer **5** could be recrystallized from tetrahydrofuran−heptane/petroleum ether, offering crystals suitable for X-ray analysis. A single crystal was mounted in air on a glass fiber. Intensity data were collected at −65 °C. A Nonius KappaCCD single-crystal diffractometer was used (φ and ω scan mode) using graphite monochromated Mo Kα radiation. 26933 reflections were measured, and 2640 ($R_{int} = 0.0679$) were unique. Unit cell dimensions were determined from the angular setting of 116 reflections. Intensity data were corrected for Lorentz and polarization effects. SADABS multiscan correction was applied.[18] The structure was solved by the program CRUNCH[19] and was refined with standard methods using SHELXL97[20] with anisotropic parameters for the non-hydrogen atoms. All hydrogens

(12) Nolte, R. J. M. *Chem. Soc. Rev.* **1994**, *23*(1), 11–19.
(13) (a) Okoshi, K.; Nagai, K.; Kajitani, T.; Sakurai, S. I.; Yashima, E. *Macromolecules* **2008**, *41*(20), 7752–7754. (b) Samori, P.; Ecker, C.; Gossl, I.; de Witte, P. A. J.; Cornelissen, J. J. L. M.; Metselaar, G. A.; Otten, M. B. J.; Rowan, A. E.; Nolte, R. J. M.; Rabe, J. P. *Macromolecules* **2002**, *35*(13), 5290–5294.
(14) (a) Cornelissen, J. J. L. M.; Donners, J. J. J. M.; de Gelder, R.; Graswinckel, W. S.; Metselaar, G. A.; Rowan, A. E.; Sommerdijk, N. A. J. M.; Nolte, R. J. M. *Science* **2001**, *293*(5530), 676–680.
(15) (a) Dabirian, R.; Palermo, V.; Liscio, A.; Schwartz, E.; Otten, M. B. J.; Finlayson, C. E.; Treossi, E.; Friend, R. H.; Calestani, G.; Mullen, K.; Nolte, R. J. M.; Rowan, A. E.; Samori, P. *J. Am. Chem. Soc.* **2009**, *131*(20), 7055–7063. (b) Schwartz, E.; Palermo, V.; Finlayson, C. E.; Huang, Y.-S.; Otten, M. B. J.; Liscio, A.; Trapani, S.; González-Valls, I.; Brocorens, P.; Cornelissen, J. J. L. M.; Peneva, K.; Müllen, K.; Spano, F.; Yartsev, A.; Westenhoff, S.; Friend, R. H.; Beljonne, D.; Nolte, R. J. M.; Samori, P.; Rowan, A. E. *Chem. Eur. J.* **2009**, *15*, 2536–2547. (c) Foster, S.; Finlayson, C. E.; Keivanidis, P. E.; Huang, Y.-S.; Hwang, I.; Otten, M. B. J.; Lu, L. L.; Schwartz, E.; Nolte, R. J. M.; Rowan, A. E. *Macromolecules*, **2009**, *42*, 2023−2030. (d) Palermo, V.; Otten, M. B. J.; Liscio, A.; Schwartz, E.; de Witte, P. A. J.; Castriciano, M. A.; Wienk, M. M.; Nolde, F.; De Luca, G.; Cornelissen, J. J. L. M.; Janssen, R. A. J.; Mullen, K.; Rowan, A. E.; Nolte, R. J. M.; Samori, P. *J. Am. Chem. Soc.* **2008**, *130*(44), 14605–14614. (e) Takei, F.; Kodama, D.; Nakamura, S.; Onitsuka, K.; Takahashi, S. *J. Polym. Sci., Part A: Polym. Chem.* **2005**, *44*(1), 585–595. (f) Garcia-Parajo, M. F.; Hernando, J.; Mosteiro, G. S.; Hoogenboom, J. P.; van Dijk, E. M. H. P.; van Hulst, N. F. *ChemPhysChem* **2005**, *6*(5), 819–827. (g) Hida, N.; Takei, F.; Onitsuka, K.; Shiga, K.; Asaoka, S.; Iyoda, T.; Takahashi, S. *Angew. Chem., Int. Ed.* **2003**, *42*(36), 4349–4352. (h) Takei, F.; Hayashi, H.; Onitsuka, K.; Kobayashi, N.; Takahashi, S. *Angew. Chem., Int. Ed.* **2001**, *40*(21), 4092–4094.
(16) (a) Beryozkina, T.; Boyko, K.; Khanduyeva, N.; Senkovskyy, V.; Horecha, M.; Oertel, U.; Simon, F.; Stamm, M.; Kiriy, A. *Angew. Chem., Int. Ed.* **2009**, *48*(15), 2695–2698. (b) Snaith, H. J.; Whiting, G. L.; Sun, B. Q.; Greenham, N. C.; Huck, W. T. S.; Friend, R. H. *Nano Lett.* **2005**, *5*(9), 1653–1657. (c) Whiting, G. L.; Snaith, H. J.; Khodabakhsh, S.; Andreasen, J. W.; Breiby, D.; Nielsen, M. M.; Greenham, N. C.; Friend, P. H.; Huck, W. T. S. *Nano Lett.* **2006**, *6*(3), 573–578.
(17) Lim, E.; Tu, G.; Schwartz, E.; Cornelissen, J. J. L. M.; Rowan, A. E.; Nolte, R. J. M.; Huck, W. T. S. *Macromolecules* **2008**, *41*(6), 1945–1951.
(18) Sheldrick, G. M. *SADABS*. Program for Emperical Absorption Correction; University of Gottingen: Germany, 1996.
(19) de Gelder, R.; de Graaff, R. A. G.; Schenk, H. *Acta Crystallogr., Sect. A* **1993**, *49*, 287–293.
(20) Sheldrick, G. M. *SHELXL-97. Program for the refinement of crystal structures*; University of Gottingen: Germany, 1997.

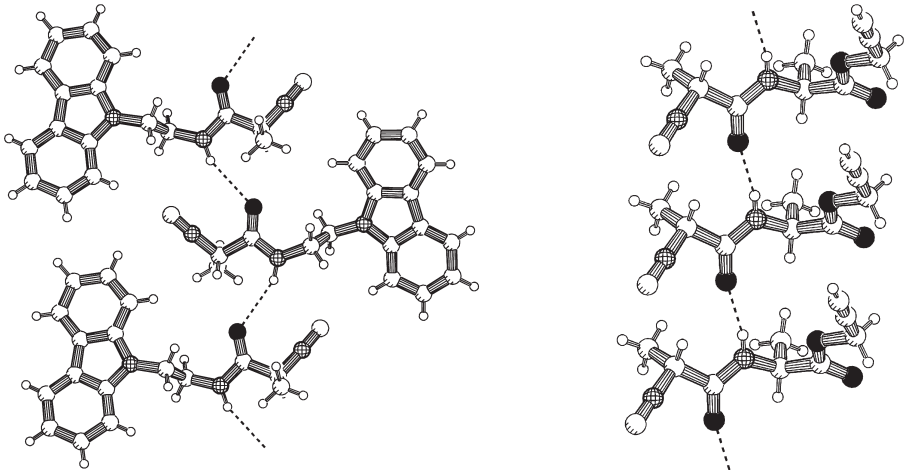

Figure 1. Molecular structure of isocyanide monomers **5** (left) and D-isocyanoalanyl-L-alanine prop-2-ynol ester (three isocyanide molecules shown).[29] In **5**, the N···O distance is 3.414(3) Å and the N−H···O angle is 155°; for D-isocyanoalanyl-L-alanine prop-2-ynol ester, these values amount to 2.843 (7) Å and 167°, respectively.

were initially placed at calculated positions and were freely refined subsequently. A PLUTON[21] drawing is shown in Figure 1.

Crystal data for **5**: translucent very light yellow-brown, $C_{18}H_{17}N_3O$, $M = 291.35$, orthorhombic, space group $P212121$, $a = 9.0264(8)$, $b = 9.9060(4)$, $c = 16.8195(10)$ Å, $\alpha = 90$, $\beta = 90$, $\gamma = 90°$, $U = 1503.92$ (17) Å^3, $T = 208(2)$ K, $Z = 4$, μ(Mo−Kα) = 0.082 mm^{-1}, 26933 reflections measured, 2640 unique (R_{int} = 0.0679), final $R1$ 0.0586, $wR2$ 0.0828 ($I > 2\sigma(I)$). More crystal data including bond lengths and angles can be found in the Supporting Information (SI).

Solid State NMR. Cross-polarization-magic angle spinning (CPMAS) spectra of monomer **5** were obtained on a Chemagnetics Infinity 300 MHz spectrometer with a Bruker 4 mm double resonance probe using a MAS speed of 7.3 kHz and 2 ms cross-polarization contact time. During CP the proton spin lock field is ramped for efficient CP transfer. Continuous phase modulation decoupling[22] of 78 kHz was applied during acquisition. CPMAS spectra of polymer **6** were obtained on a Varian VNMRS 600 MHz spectrometer using a MAS speed of 14 kHz with a CP contact time of 1.5 ms and a two pulse phase modulation (TPPM)[23] of 78 kHz rf field strength was applied during acquisition. The proton spin lock field is ramped for efficient CP transfer. Single-pulse proton NMR spectra were recorded with MAS frequency of 40 kHz on a Chemagnetics Infinity 600 MHz spectrometer with a Varian 1.6 mm triple resonance probe.

Immobilization of Ni(II) Catalyst and Preparation of the Polyisocyanide Layer on Substrates. The carbazole functionalized brushes were prepared in a similar way as the LL-PIAA brushes reported recently.[17] In short, the plasma-cleaned silicon wafer was immersed into a solution of 4 mM Ni(II) catalyst (6 mg, 0.008 mmol) in dichloromethane (2 mL). The substrates were rinsed thoroughly with chloroform to remove any non-bound catalyst, and dried with nitrogen. Subsequently, the polyisocyanide layer was prepared by placing the catalyst-modified substrates in a solution of **5** in dichloromethane (1.5 mL). Finally, the substrate was washed with chloroform and methanol and dried with nitrogen.

Film thicknesses were measured using a J. A. Woollam alpha SE ellipsometer using a Cauchy model. Height-mode atomic force microscopy (AFM) images were obtained using a Digital Instruments Nanoscope III, in tapping mode. The root-mean-square (rms) surface roughness of brushes was obtained from AFM images. Contact angle measurements were performed using a homemade stage with a computer-controlled micro-syringe and a digital camera. An infusion rate of 2 L/min was used, and images for advancing angles were recorded.

Electroabsorption. Electroabsorption measurements were performed in vacuum on a home-built system with a probing beam at 515 nm, which is at the low-energy edge of the F8BT absorption band. The AC voltage superimposed on the DC bias to enable measurement of $\Delta T/T$ had a peak-to-peak amplitude of 0.5 V at a frequency of 2 kHz.

Submicroscopic Kelvin Probe Force Microscopy (KPFM). The KPFM measurements have been performed by employing a commercial microscope Multimode (Veeco) with Extender Electronics module. In order to obtain a sufficiently large and detectable mechanical deflection, we used (k = 2.8 N/m) Pt/Ir coated Si ultra levers (SCM, Veeco) with oscillating frequencies in the range $60 < \omega < 90$ kHz. Both sides of the cantilever are coated with 20 nm of Pt/Ir, with a buffer layer (3 nm) of Cr to improve the adhesion. AFM and KPFM images are acquired in the same measurement, a topographic line scan is first obtained by AFM operating in tapping mode and then that same line is rescanned in lift mode with the tip raised to a lift height of 50 nm. The work function of the used tip has been obtained by calibration with respect to freshly cleaved highly oriented pyrolitic graphite (HOPG).

Macroscopic Kelvin Probe. Macroscopic Kelvin probe measurements were performed on a Kelvin Control 07 system (Besocke Delta Phi GmbH) with a gold mesh probe (Kelvin Probe S, Besocke Delta Phi GmbH) with a diameter of 6 mm. Calibration of the probe was performed against a freshly cleaved HOPG surface. A comprehensive description of the technique can be found in the work of Palermo and co-workers[24] and references therein.

Compounds. *N*-(2-aminoethyl)carbazole **1**[25] and the Nickel(II) catalyst[17] were prepared according to literature procedures.

(21) Spek, A. L. *PLATON, A Multipurpose Crystallographic Tool*; Utrecht University: Utrecht, The Netherlands, 2004.
(22) De Paepe, G.; Elena, B.; Emsley, L. *J. Chem. Phys.* **2004**, *121*(7), 3165–3180.
(23) Bennett, A. E.; Rienstra, C. M.; Auger, M.; Lakshmi, K. V.; Griffin, R. G. *J. Chem. Phys.* **1995**, *103*(16), 6951–6958.
(24) Palermo, V.; Palma, M.; Samori, P. *Adv. Mater.* **2006**, *18*(2), 145–164.
(25) Conn, M. M.; Deslongchamps, G.; de Mendoza, J.; Rebek, J. *J. Am. Chem. Soc.* **1993**, *115*(9), 3548–3557.

The numbering scheme used for the assignment of the chemical shifts in the NMR spectra of the carbazole compounds is shown in Figure S10 (of the Supporting Information).

Boc-L-alanine 2-(9*H*-Carbazole-9-yl) Ethyl Amide 2. *N*-(2-aminoethyl)carbazole (2.00 g, 9.5 mmol) and Boc-L-Ala-OH (1.98 g, 10.5 mmol) were dissolved in CH_2Cl_2 (300 mL). To this solution, diisopropylethylamine (DIPEA; 1.79 mL, 10.4 mmol, 1.1 equiv), 1-hydroxybenzatriazole (HOBt; 1.60 g, 10.4 mmol, 1.1 equiv), and 1-(3-dimethylaminopropyl)-3-ethylcarbodiimide hydrochloride (EDC; 2.00 g, 10.4 mmol, 1.1 equiv) were subsequently added. After stirring for 3 h, the CH_2Cl_2 solution was washed, first with an aqueous 10% (w/w) citric acid solution (2 × 300 mL), followed by H_2O (300 mL), an aqueous 10% (w/w) sodium carbonate solution (2 × 300 mL), and again by H_2O (300 mL). The organic layer was dried (Na_2SO_4), concentrated, and subjected to column chromatography (1% MeOH in $CHCl_3$), yielding 80% of **2** as a white powder. Mp 195 °C. $[\alpha]_D = -6$ (*c* 1.1, THF). ^{1}H NMR (δ ppm, $CDCl_3$, 300 MHz): 8.10 (d, $J = 7.8$ Hz, 2H, H_4,), 7.45 (m, 2H, H_1), 7.24 (m, 4H, $H_2 + H_3$), 6.14 (br s, 1H, NH), 4.51 (m, 2H, NCH_2), 4.01 (qn, $J = 6.9$ Hz, 1H, CH Ala,), 3.71 (m, 2H, CH_2NH), 1.36 (s, 9H, $C(CH_3)_3$), 1.24 (d, $J = 6.9$ Hz, 3H, CH_3 Ala,). ^{13}C NMR (δ ppm, $CDCl_3$, 75 MHz): 173.3, 154.8 (C=O), 140.3 (C_1), 126.0 (C_3), 123.1 (C_6), 120.6 (C_5), 119.4 (C_4), 108.8 (C_2), 80.2 ($C(CH_3)_3$), 68.1 (CH Ala), 41.9 (NCH_2), 38.8 (CH_2NH), 28.4 ($C(CH_3)_3$), 18.1 (CH_3 Ala). FT-IR (cm^{-1}, ATR): 3346, 3330 (NH), 1697 (amide I), 1655 (C=C), 1545 (amide II). MS-ESI: $m/z = 404$ $[M + Na]^+$. HRMS for $C_{22}H_{27}N_3O_3Na$: calcd 404.1950, found 404.1951.

***N*-Formyl-L-alanine 2-(9*H*-Carbazole-9-yl) Ethyl Amide 4.** The Boc-protecting group of **2** (2.0 g, 5.2 mmol) was removed by dissolving **2** in HCl-saturated ethyl acetate (150 mL). The mixture was stirred for 12 h after which time the solvent was evaporated in vacuo and the excess HCl was removed by addition of *t*-BuOH/CH_2Cl_2 and subsequent evaporation. The resulting HCl salt **3** was taken up in ethyl formate (300 mL) and sodium formate (2.3 g, 33.8 mmol, 6.5 equiv) was added. The mixture was stirred under reflux for 21 h before the solid was filtered off and washed thoroughly with $CHCl_3$. The solvent was removed from the filtrate, and the crude product was recrystallized two times from THF/diisopropyl ether to give 1.1 g (48%) of white solid. Mp 221 °C. $[\alpha]_D = -32$ (*c* 1.1, DMSO). ^{1}H NMR (δ ppm, DMSO-d_6, 300 MHz): 8.16 (br, 1H, NH), 8.13 (d, $J = 7.8$ Hz, 2H, H_4,), 7.93 (s, 1H, HCO), 7.57 (d, $J = 8.1$ Hz, 2H, H_1), 7.43 (t, $J = 7.2$ Hz, 2H, H_3), 7.19 (t, $J = 7.2$ Hz, 2H, H_2), 4.43 (t, $J = 6.3$ Hz, 1H, NCH_2), 4.17 (qn, $J = 6.9$ Hz, 1H, CH Ala), 3.57 (m, 2H, CH_2NH), 0.99 (d, 3H, CH_3 Ala, $J = 6.9$ Hz). ^{13}C NMR (δ ppm, DMSO-d_6, 75 MHz): 172.3 (C=O), 160.8 (HCO), 140.2 (C_1), 125.8 (C_3), 122.2 (C_6), 120.3 (C_5), 119.0 (C_4), 109.2 (C_2), 46.9 (CH Ala), 41.6 (NCH_2), 38.0 (CH_2NH), 18.2 (CH_3 Ala). FT-IR (cm^{-1}, ATR): 3285 (NH), 1658 (amide I), 1631 (C=C), 1562 (amide II). MS-ESI: $m/z = 332$ $[M + Na]^+$. HRMS for $C_{18}H_{19}N_3O_2Na$: calcd 332.1375, found 332.1371. Anal. calcd for $C_{18}H_{19}N_3O_2$: C, 69.88; H, 6.19; N, 13.58. Found: C, 69.85; H, 6.19; N, 13.19.

L-Isocyanoalanine 2-(9*H*-Carbazole-9-yl) Ethyl Amide 5. Compound **4** (0.94 g, 3.0 mmol) was dissolved in THF/$CHCl_3$ (400 mL 3:1 v/v) under an N_2 atmosphere and *N*-methyl morpholine (1.5 mL, 13.6 mmol, 4.5 equiv) was added. The resulting solution was cooled to −30 °C (acetone/CO_2) and diphosgene (0.3 mL, 2.5 mmol, 0.8 equiv) in $CHCl_3$ (20 mL) was added dropwise to over a period of 15 min, while the temperature was maintained at −30 °C. After complete addition of diphosgene, the orange solution was allowed to warm to 0 °C and an ice-cold saturated aqueous sodium bicarbonate solution (50 mL) was added and stirred vigorously for 10 min. The product was extracted with $CHCl_3$ (100 mL) and subsequently washed with an aqueous 10% (w/w) sodium bicarbonate solution and water (50 mL). The organic layer was dried (Na_2SO_4) and evaporated in vacuo resulting in a yellow-orange solid. The product was purified using column chromatography (THF/heptane 9:1 v/v) and subsequently recrystallized two times from tetrahydrofuran−heptane/petroleumether to yield **5** as yellow crystals (380 mg, 43%). Mp 166 °C. $[\alpha]_D = 23$ (*c* 1.1, THF). ^{1}H NMR (δ ppm, DMSO-d_6, 300 MHz): 8.37 (t, $J = 6.3$ Hz, 1H, NH), 8.14 (d, $J = 7.5$ Hz, 2H, H_4), 7.58 (d, $J = 8.1$ Hz, 2H, H_1), 7.44 (t, $J = 6.9$ Hz, 2H, H_3), 7.20 (t, $J = 7.8$ Hz, 2H, H_2), 4.49 (t, $J = 6.3$ Hz, 1H, NCH_2), 4.25 (q, $J = 6.9$ Hz, 1H, CH Ala), 3.54 (m, 2H, CH_2NH), 1.21 (d, $J = 6.9$ Hz, 3H, CH_3 Ala). ^{13}C NMR (δ ppm, DMSO-d_6, 75 MHz): 166.6 (C=O), 159.8 (CN), 140.1 (C_1), 125.7 (C_3), 122.1 (C_6), 120.2 (C_5), 118.8 (C_4), 109.0 (C_2), 52.2 (CH Ala), 41.2 (NCH_2), 38.3 (CH_2NH), 19.1 (CH_3 Ala). FT-IR (cm^{-1}, ATR): 3311 (NH), 2164 + 2148 (CN), 1681, 1669 (amide I, C=C), 1557 (amide II). MS-ESI: $m/z = 314$ $[M + Na]^+$. HRMS for $C_{18}H_{17}N_3O_1Na$: calcd 314.1269, found 314.1269. Anal. calcd for $C_{18}H_{17}N_3O_1$: C, 74.20; H, 5.88; N, 14.42. Found: C, 74.11; H, 5.79; N, 14.12.

UV−vis ($CHCl_3$) λ_{max}, nm (ε): 264 (20146), 294 (19060), 329 (4978), 343 (5368, mol^{-1} L cm^{-1}). Fluorescence ($CHCl_3$, $\lambda_{exc} = 294$ nm) λ_{max}, nm: 351 and 366.

Poly(L-Isocyanoalanine 2-(9*H*-Carbazole-9-yl) Ethyl Amide) 6. To a stirred solution of **5** (115 mg, 0.41 mmol) in $CHCl_3$ (25 mL) was added $Ni(ClO_4)_2 \cdot 6H_2O$ (0.01 equiv.; 8 μL of a 0.53 M MeOH solution). The solution immediately turned yellow/orange and was stirred for 5 min before the polymer precipitated. The off-white polymer was filtered off and washed extensively with MeOH. Drying in vacuo gave the polymer as an off-white solid in 86% yield. FT-IR (cm^{-1}, KBr): 3265 (NH), 1654 (amide I), 1532 (amide II). Anal. calcd for $C_{18}H_{17}N_3O$: C, 74.20; H, 5.88; N, 14.42. Found: C, 73.89; H, 6.06; N, 14.11.

3. Results and Discussion

3.1. Synthesis of Monomer and Polymer. The synthetic route to the carbazole functionalized polyisocyanide is outlined in Scheme 1. First, *N*-(2-aminoethyl)carbazole[25] **1** was coupled to Boc-L-Ala-OH using 1-(3-dimethylaminopropyl)-3-ethyl carbodiimide hydrochloride (EDC) and 1-hydroxybenzatriazole (HOBt) to give **2**. The formamide **4** was obtained by cleavage of the Boc-protecting group of **2** with an HCl-saturated solution of ethyl acetate, followed by refluxing of the resulting amine salt **3** in ethylformate in the presence of sodium formate. Dehydration of formamide **4** with diphosgene and *N*-methylmorpholine (NMM) resulted in the formation of isocyanide monomer **5**. The isocyanide monomer was purified by column chromatography and recrystallized from tetrahydrofuran−heptane/petroleum ether, offering light yellow-brown crystals suitable for X-ray analysis (Figure 1). The X-ray has established the conformation and relative stereochemistry of **5**, which crystallizes in the orthorhombic system, space group $P2_12_12_1$, with four molecules in the unit cell. Analogous to related isocyanides (for example l-isocyanoalanyl-L-alanine methyl ester[14] or D-isocyanoalanyl-L-alanine prop-2-ynol ester[20]) a hydrogen bonding array was found between stacked molecules of **5**. Molecules of **5** are linked by N−H···O=C hydrogen bonds in the

Scheme 1. Synthesis of Polymer 6[a]

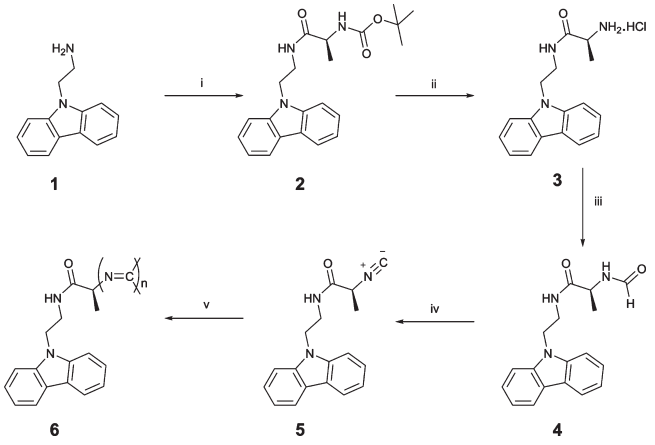

[a] Reagents and reaction conditions: (i) Boc-L-Ala-OH, EDC, HOBt, CH_2Cl_2, 80%; (ii) EtOAc·HCl/^{t}BuOH; (iii) ethyl formate, $NaHCO_2$, reflux, 46% ; (iv) diphosgene, *N*-methylmorpholine, CH_2Cl_2, −30°C, 43%; (v) 0.01 equiv $Ni(ClO_4)_2 \cdot 6H_2O$, CH_2Cl_2, 86%.

b-direction, with an N···O distance of 3.414(3) Å and an N−H···O=C angle of 155°. The hydrogen bonding interactions are longer and, hence, weaker than for the related isocyanides. In reference to the above observation, we have analyzed, using solid state NMR spectroscopy, the solid state NH proton chemical shifts since it is well-known that the amide protons show downfield shifts with decreasing hydrogen bond lengths.[26] The L-isocyanoalanyl-L-alanine methyl ester isocyanide monomer has an N−H···O=C hydrogen bonding and a NH proton shift of $\delta = 9.6$ ppm in the solid state.[27] In the present monomer **5**, however, the NH proton shift of $\delta = 5.4$ ppm is rather upfield, which could be due to a combination of hydrogen bonding and shielding effects of the carbazole ring. A detailed analysis is currently underway to analyze the individual contributions.[28] In contrast to the isocyanide molecules of D-isocyanoalanyl-L-alanine prop-2-ynol ester, which stacks in a single hydrogen-bonding array (Figure 1, right), molecule **5** stacks in an interdigitated arrangement. Most likely, the carbazole moiety introduces sufficient steric bulk hindrance and prevents a similar ordering.

The absorption spectrum of **5** in chloroform shows vibronic bands at $\lambda = 264$, 294, 329, and 343 nm (Figure S1 (of the Supporting Information)). The last two peaks are attributed to the $\pi \rightarrow \pi^*$ and the $n \rightarrow \pi^*$ transitions of the carbazole ring, respectively. Upon excitation at the absorption maximum of $\lambda = 294$ nm, the isocyanide monomer shows an emission profile with a weak band at $\lambda = 351$ nm and a more pronounced band at $\lambda = 366$ nm (Figure S1).

Isocyanide **5** was polymerized with 1 mol% $Ni(ClO_4)_2 \cdot 6H_2O$ in dichloromethane, in the presence of which the originally colorless solution rapidly turned yellow/orange. After stirring for 5 min, polymer **6** precipitated from the solution. The off-white precipitate was filtered off and washed extensively with methanol and subsequently dried, offering a cream solid. The polymer was found to be insoluble in most organic solvents. To obtain greater insight into the structures of the polymers, the polymerization of **5** in $CHCl_3$ with $Ni((ClO)_4)_2$ as a catalyst (1/30 equiv) was monitored by infrared spectroscopy (Figure S2 (of the Supporting Information)). Most characteristic for the polymerization is the disappearance of the isocyanide peak at $\nu = 2142$ cm^{-1}, and from this signal, the reaction was determined to be completely finished after ~600 s. Upon polymerization of isocyanopeptides the NH-stretching vibration and the amide I vibration shift to lower wavenumbers, as is expected when hydrogen bonds are formed between the amide groups in the side chain. The shift of the N−H stretching vibration from $\nu = 3446$ to 3265 cm^{-1} and the shift of the amide I vibrations from $\nu = 1688$ to 1652 cm^{-1} confirm the presence of a hydrogen-bonding network, and these shifts are comparable with the polymerization of L-isocyanoalanyl-L-alanine methyl ester[30] and D-isocyanoalanyl-L-alanine prop-2-ynol ester.[29] The polymerization was found to occur rapidly in dichloromethane, chloroform, tetrachloroethane, and tetrachlorethane/1,2-dichlorobenzene (1:1 v/v); the monomer was consumed within 10 min, and the polymer could be seen as a precipitate in the cuvette. In each of these solvents, the differences observed in the N−H stretching and amide I vibrational shifts are similar. Tetrahydrofuran showed a significantly slower rate of polymerization of **5** (>2 h) and less pronounced shifts of the N−H stretching, and amide I vibrations were observed in the IR spectrum of the polymer. This observation can be rationalized by the higher polarity of solvents such as tetrahydrofuran, which will hamper the formation of the hydrogen bonding network.[31]

Due to the insolubility of **6**, characterization was carried out using IR and solid state NMR spectroscopies and differential scanning calorimetry (DSC). The solid state IR spectrum of **6** (Figure S3 (of the Supporting Information)) revealed the complete disappearance of the CN stretching vibration at $\nu = 2164$ and 2148 cm^{-1} and the shift of the N−H stretching and amide I vibrational characteristic of hydrogen bonding between the amides. DSC analysis of **6** did not show any melting or glass transition in the range from 20 to 250 °C, reflecting the stable and rigid nature of this polymer. Elemental analysis of the polymer indicated that the polymer was

(26) (a) Yamauchi, K.; Kuroki, S.; Fujii, K.; Ando, I. *Chem. Phys. Lett.* **2000**, *324*(5−6), 435–439. (b) Jeffrey, G. A. *An Introduction to Hydrogen Bonding*; Oxford University Press: New York, 1997.
(27) Cornelissen, J. J. L. M.; Graswinckel, W. S.; Adams, P. J. H. M.; Nachtegaal, G. H.; Kentgens, A. P. M.; Sommerdijk, N. A. J. M.; Nolte, R. J. M. *J. Polym. Sci., Part A: Polym. Chem.* **2001**, *39*(24), 4255–4264.
(28) Gowda, C. M.; Schwartz, E.; van Eck, E. R. H.; Brinkmann, A.; de Wijs, G.; Kresse, G.; Marsman, M.; De Gelder, R.; Cornelissen, J. J. L. M.; Nolte, R. J. M.; Rowan, A. E.; Kentgens, A. P. M., manuscript in preparation.
(29) Schwartz, E.; Kitto, H. J.; de Gelder, R.; Nolte, R. J. M.; Rowan, A. E.; Cornelissen, J. J. L. M. *J. Mater. Chem.* **2007**, *17*(19), 1876–1884.
(30) Cornelissen, J. J. L. M.; Donners, J. J. J. M.; de Gelder, R.; Graswinckel, W. S.; Metselaar, G. A.; Rowan, A. E.; Sommerdijk, N. A.; Nolte, R. J. M. *Science* **2001**, *293*(5530), 676–80.
(31) Kajitani, T.; Okoshi, K.; Yashima, E. *Macromolecules* **2008**, *41*(5), 1601–1611.

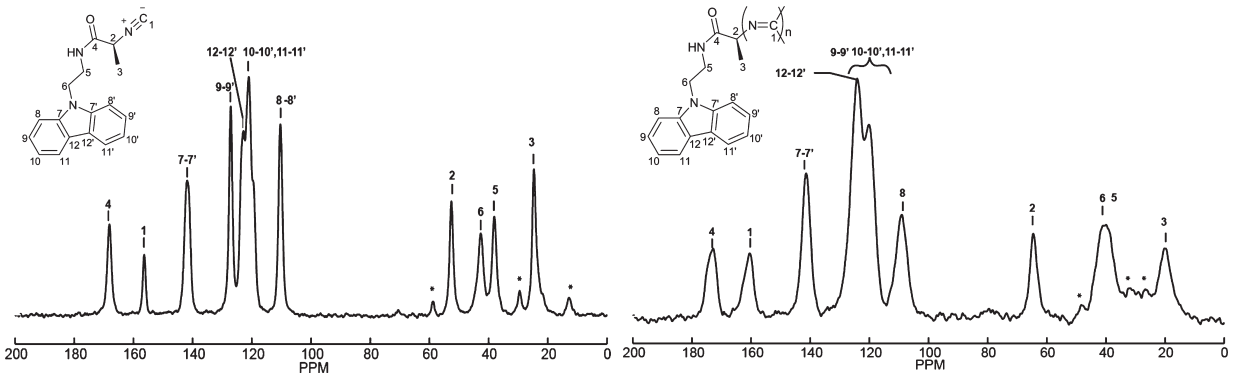

Figure 2. Cross-polarization−magic angle spinning spectra of monomer **5** (left) and polymer **6** (right) shown along with the assignments. The inset shows the numbering used for the assignment of the chemical shifts in the ^{13}C NMR spectra. The asterisks denote the spinning sidebands.

obtained with satisfactory purity (see the Experimental Section).

3.2. Solid State NMR Characterization of the Monomer 5 and Polymer 6. Hartman−Hahn cross-polarization (CP) solid state NMR spectroscopy in combination with magic angle spinning (MAS) and dipolar decoupling with RF pulse irradiation techniques were used to obtain high-resolution solid state NMR spectra.[32]

^{13}C NMR Spectroscopy. Figure 2 shows the one-dimensional ^{13}C CPMAS spectra of the monomer **5** and the polymer **6** acquired using the pulse sequence shown in Figure S4 (of the Supporting Information). The spectra are referenced to the CH_2 carbon peak of adamantane at $\delta = 38.48$ ppm. The carbon resonances in the monomer are narrower than those of the polymer. The resonance at $\delta = 24.4$ ppm (C_3) in the monomer has a width at half height of 105 Hz and the corresponding resonance at $\delta =$ 20 ppm in the polymer has a line width of 760 Hz; both of these resonances correspond to the CH_3 group. The monomer is crystalline in nature and exhibits sharp lines, whereas the polymer apparently lacks long-range order and as a result shows dispersion in shifts. The aliphatic carbons appear between $\delta = 10-70$ ppm, the aromatic carbons appear between $\delta = 100-145$ ppm, the carbonyl (4), the isocyano (1, C≡N), and the imine (1, C=N) carbons are more downfield shifted and appear above $\delta = 150$ ppm in the monomer and the polymer. The total number of carbon lines of the monomer spectrum in Figure 2 does not exceed the number of carbon sites in the molecule, which indicates that the monomer has one molecule per asymmetric unit cell, as also confirmed by X-ray crystallography. The wider line widths of the carbon resonances in the region between $\delta = 100-132$ ppm results in considerable overlap for the polymer; hence, it displays fewer lines than the monomer.

^{1}H NMR Spectroscopy. In Figure S4 (of the Supporting Information), the fast ^{1}H MAS single pulse ^{1}H NMR spectra of the monomer **5** and the polymer **6** are displayed. The broad profile of proton resonances arises due to the large homonuclear dipolar couplings experienced by the protons. The chemical shift assignment of the compounds was done by applying various solid state NMR methodologies.[28] The assignments thus obtained are tabulated in Table 1 for the monomer and the polymer.

Table 1. ^{13}C and ^{1}H Chemical Shifts of the Monomer 5 and the Polymer 6 in the Solid State

carbon site		monomer ppm	polymer ppm
1C	CN	155.8	160.0
2C	CH	52.2	64.5
3C	CH_3	24.4	20.0
4C	C=O	167.7	172.6
5C	CH_2	37.7	40.1
6C	CH_2	42.4	41.4
7C-7′C	ring	141.0, 141.8	140.8
8C-8′C	ring	109.9	108.6
9C-9′C	ring	126.8	123.6, 119.8 (unresolved)
10C-10′C	ring	121.0, 119.0[a]	
11C-11′C	ring	121.0, 120.2[a]	
12C-12′C	ring	123.2, 122.5	123.8

proton site		monomer ppm	polymer ppm
3H	CH_3	1.2	0.6
2H	CH	2.7	4.4
5H	CH_2	3.2	3.7, 4.0
6H	CH_2	3.5	
8H-8′H	ring	7.4, 8.1	7.0
9H-9′H	ring	7.6	7.1, 7.2
10H-10′H	ring	7.3, 4.7[a]	
11H-11′H	ring	7.6, 5.8[a]	
NH		5.4	8.1

[a] The shifts correspond to the unprimed and primed positions in these cases, respectively.

The pronounced differences in the ^{1}H NMR chemical shifts of the monomer **5** and the polymer **6,** at the aromatic and alanine moieties, indicate differences in the arrangement of the side chains of **5** and **6**. The ^{13}C resonances in the carbazole ring of the polymer **6** are limited in resolution, which hamper easy analysis; nevertheless, small changes in the shifts are evident. The clear shifts of the alanine moiety are indicative of a hydrogen bonding network formed upon polymerization. A detailed analysis of ^{1}H and ^{13}C shifts correlating chemical shifts to the structures of **5** and **6** are discussed elsewhere in detail.[28]

3.3. Synthesis of Carbazole Functionalized Brushes. The previous polymerization in solution resulted in insoluble polymers; hence, monomer **5** was polymerized from the surface to give brush layers of **6**. A similar approach as previously demonstrated for the LL-PIAA

(32) Hartmann, S. R.; Hahn, E. L. *Phys. Rev.* **1962**, *128*(5), 2042–2053.

Scheme 2. Procedure for the Surface-Initiated Polymerization of 5[a]

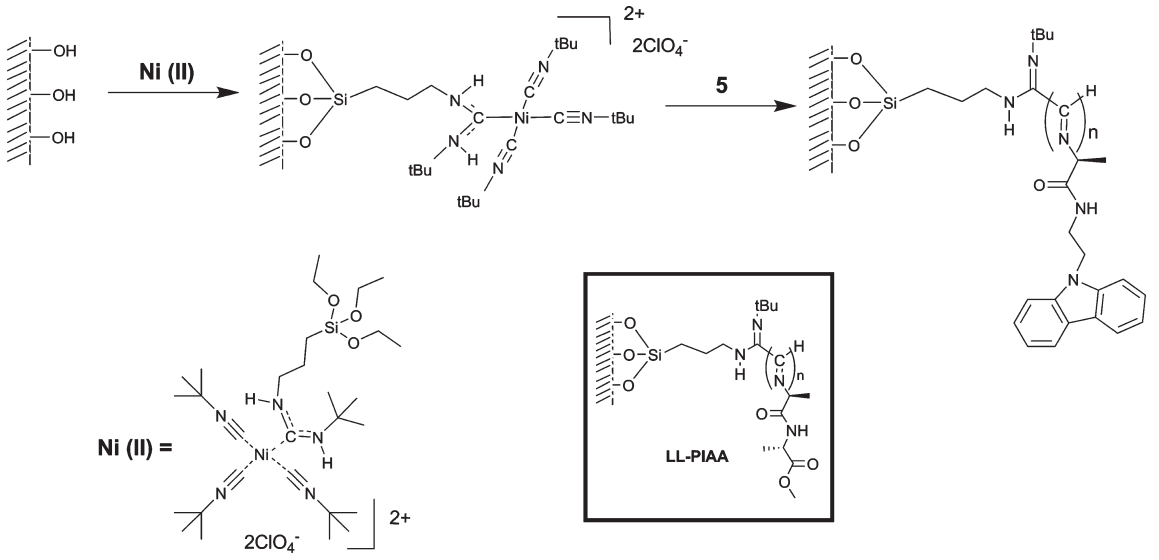

[a] The inset shows the LL-PIAA brush for comparison.[17]

brushes was used.[17] A triethoxysilane carbene-like Ni(II) catalyst was used to create Ni-functionalized SAMs on Si/SiO_2 surfaces offering an activated platform for the efficient initiation and growth of the polyisocyanide brushes (Scheme 2). Within 2 h, brushes up to 150 nm could be obtained. The water contact angles for the brush were found to be around 90°, which is slightly higher than observed for the LL-PIAA brush (72°), which is attributed to the more hydrophobic carbazole moiety.

The surface-initiated polymerization of **5** could be controlled by changing the monomer concentration, the solvent, and the polymerization reaction time (Figure 3 and Table 2). The initial hour of the polymerization shows a nearly linear relationship between polymer growth vs time. At later stages of the polymerization, the growth is no longer linear, which is ascribed to termination processes and chain transfer processes and is often observed in brush polymerizations.[33] The influence of different solvents on the brush growth is clearly visible from Figure 3. In CH_2Cl_2, the polymerization of **5** proceeds rapidly and brushes with a thickness of 150 nm for a 48 mM solution are obtained in 2 h. In agreement with polymerization studies of the monomer **5** in solution (as followed by IR, vide supra), THF seemed to be a less ideal solvent for the polymerization of **5**. Using higher monomer concentrations, thicker brushes for the same reaction time and solvent could be obtained (48 vs 16 mM yields 150 vs 50 nm, respectively).

The AFM morphology of the polycarbazole brushes (on Si) is shown in Figure 4 and Figure S6 (of the Supporting Information). The film morphologies varied by film thickness; thin (~9 nm) brushes show a mosslike appearance with a roughness root-mean-square (R_{rms}) value of 1.9 nm, whereas in thicker brushes, a more fiberlike architecture with R_{rms} values of around 4 nm is observed. The thicker films have, in general, rougher surfaces and, in some cases, bulk polymers could be found on top of the brush films. The specific fiberlike structure

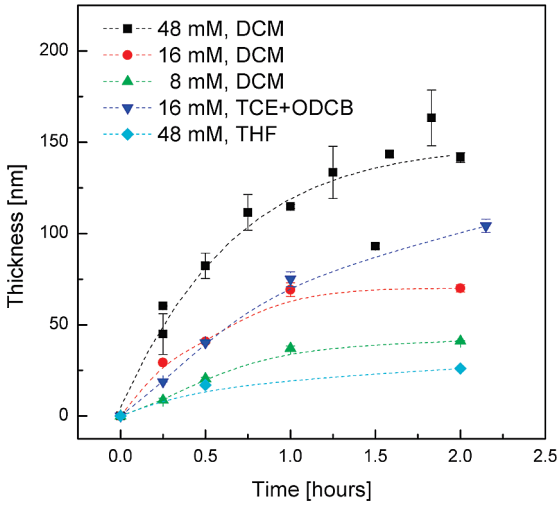

Figure 3. Film thickness as a function of polymerization time for different concentration of the monomer and various solvents. DCM dichloromethane; TCE trichloroethane; ODCB *ortho*-dichlorobenzene; THF tetrahydrofuran. The thicknesses were obtained using ellipsometry.

Table 2. Film Thickness of Polymer Brushes from Various Reaction Time, Solvent for Monomer, and Monomer Concentrations[a]

	thickness [nm][b]				
	DCM			TCE:ODCB[c]	THF
polymerization time [min][a]	48 mM[d]	16 mM[d]	8 mM[d]	16 mM[d]	48 mM[d]
15	60.3 ± 0.3	29.3 ± 0.7	8.7 ± 1.1	18.3 ± 0.1	
30	82.3 ± 6.9	40.8 ± 0.5	20.5 ± 0.7	40.2 ± 0.3	17 ± 1.0
60	114.8 ± 1.1	69.2 ± 3.8	37.1 ± 1.3	75.0 ± 4.0	
120	141.6 ± 2.7	70 ± 2.0	41.1 ± 0.2	104.2 ± 3.7	26 ± 3.7

[a] Polymerization time after the immobilization of catalyst complex. [b] Average values for separate brush samples prepared using the same conditions and from at least three spots on each sample. [c] TCE:ODCB = 1:1 (v/v). [d] Monomer concentration (48 mM = 14 mg of monomer in 1 mL of solvent).

(33) Jones, D. M.; Huck, W. T. S. *Adv. Mater.* **2001**, *13*(16), 1256–1259.

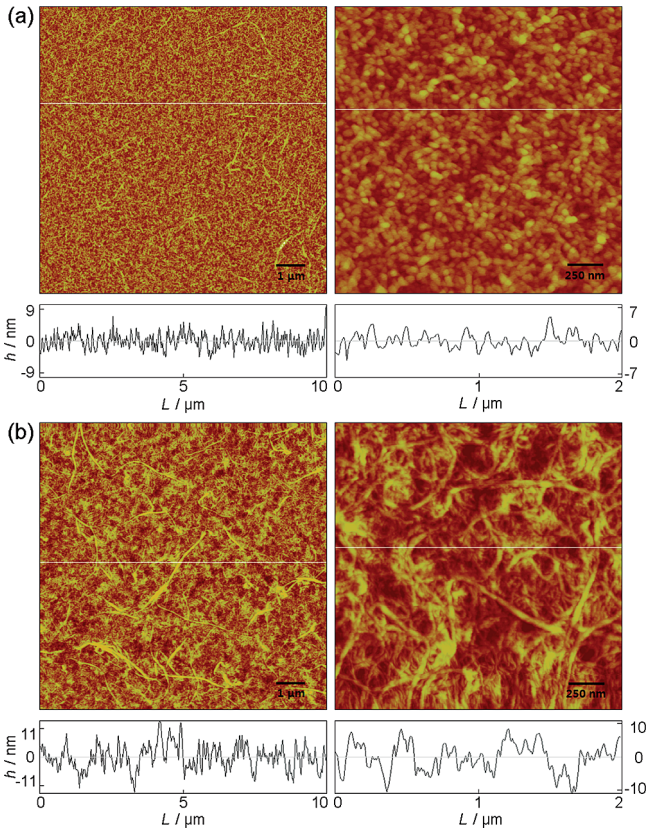

Figure 4. AFM morphology of carbazole polymer brushes grown on a silicon wafer with film thicknesses of (a) 9 (R_{rms} = 2.2 (left) and 1.9 (right)) and (b) 73 nm (R_{rms} = 6.3 (left) and 4.1 (right)). Scan size for a 10 × 10 μm^2 and for b 2 × 2 μm^2, respectively.

can result in large interfacial areas, which can be beneficial for organic electronic devices.

It should be noted that the brushes are probably of rather low grafting density, as the AFM images show a rather "open" structure. However, due to the insoluble nature of the polymers, we have not attempted to compare molecular weights of polymers on the surface and in solution, and hence, no grafting density can be determined

The UV−vis spectrum of the polymer brush shows similar vibronic bands between λ = 250−350 nm as for the monomer (Figure S7 (of the Supporting Information)). The spectrum is broader, which is general for solid state spectra as compared to solution spectra. In addition, the maxima of all vibronic bands were red-shifted by λ = 2−6 nm, which indicates an increased interaction between the carbazole moieties. Similar observations were reported for polyacetylenes with carbazole side groups.[5]

We also studied the brush films with circular dichroism (CD) spectroscopy. It is expected that the helical conformation of the polyisocyanides is also translated to the properties of the polymer brush. For polyisocyanides the $n-\pi^*$ transition of the imine chromophore, residing in the wavelength range from λ = 250−350 nm, can be monitored in the CD spectrum. Because an optically pure L-alanine unit was built into the polymer, we expect a similar CD signal for the carbazole brush as was observed for the LL-PIAA brush.[17] Indeed, a positive Cotton effect centered around λ = 310 nm is observed (Figure S8 (of the Supporting Information)), indicating the formation of right-handed helical structures on the brush.[34] The additional CD signals around λ = 300 and 350 nm might originate from the carbazole moieties. A comparison with the bulk polymer **6** was, however, not possible due to a lack of solubility of **6**.

To obtain a final indication that the polymer brushes of **6** have similar properties to those of the bulk polymer, (solid state) IR spectroscopic measurements were carried out. Similar shifts (from ν = 3377 and 1683 cm^{-1} to ν = 3265 and 1655 cm^{-1}, for the NH and amide I vibrations, respectively) compared to monomer **5** were found for both the bulk polymer as well as the brush of **6**; although the IR spectrum of the carbazole polymer brush is sufficiently broadened, the main characteristic features and signals are similar; this confirms that the hydrogen bonding arrays which exist between the side chains of the polymer brushes occurs both in the solid state of the bulk polymer and in the polymer brush (Figure S9 and Table S2 (of the Supporting Information)).

3.4. Kelvin Probe and Kelvin Probe Force Microscopy. It is expected that a dipole in vertically aligned polymer brushes grown on electrodes might significantly alter the work function of the underlying electrode. This change in work function can be quantified by KP and KPFM techniques.[24,35] We focused our attention onto polymer films with a thickness of a few tens of nanometers, supported on either ITO or silicon, for KP or KPFM studies, respectively.

Different terms can be expected to contribute to the work function (WF) of a surface exposing the polymer brushes as measured by Kelvin probe techniques, including the following: (i) the potential of the substrate, (ii) the dipolar character of the carbazole polymer brushes films, and (iii) the dipoles at the substrate−polymer interface, which can be neglected for films thicker than 10 nm. The dipoles contribution of the carbazole polymers to the WF of the system can be directly quantified by using the clean substrate surface as reference (i.e., $\Delta WF = WF_{sample} - WF_{substrate} = -\mu/\varepsilon$), where ε and μ represent the dielectric constant and the perpendicular component of the effective dipole moment of the brush film, taking into account the packing of the polymers, their polarizability as well as the depolarizing effects. For films grown on silicon, given the ultra flat nature of the substrate (i.e., having a roughness measured with AFM of fractions of angstroms, thus being close to the noise level), the geometrical arrangement of the dipoles depends to a great extent on the conformation adopted by the polymeric brushes. For films grown on ITO, the KP technique allows measurement of the WF modification on realistic electrodes, although the average roughness of the substrate is of the order of 2−3 nm.

(34) Cornelissen, J. J. L. M.; Graswinckel, W. S.; Rowan, A. E.; Sommerdijk, N. A. J. M.; Nolte, R. J. M. *J. Polym. Sci., Part A: Polym. Chem.* **2003**, *41*(11), 1725–1736.
(35) Saito, N.; Hayashi, K.; Sugimura, H.; Takai, O.; Nakagiri, N. *Surf. Interface Anal.* **2002**, *34*(1), 601–605.

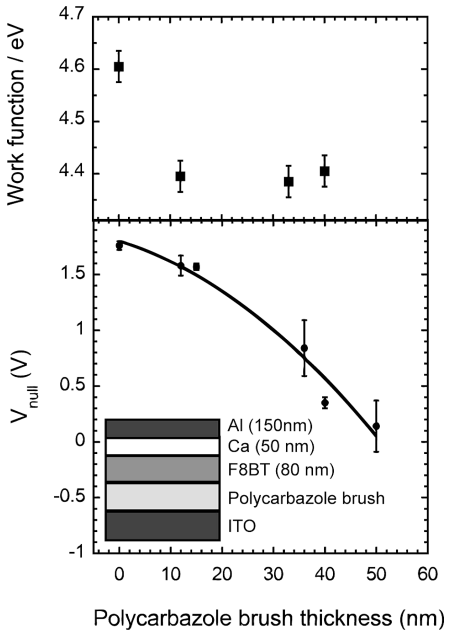

Figure 5. (top) Work function measurements performed by macroscopic Kelvin probe (KP) on carbazole functionalized brushes grown in situ on ITO substrates. (bottom) Electroabsorption measurement of the null voltage in sandwich devices incorporating carbazole polymer brush layers. The null voltage is obtained by extrapolating from the linear region of the electroabsorption data depicted in Figure 6 at low bias voltage.

In Figure 5, top panel, the work function variation of brushes grown on ITO electrodes at various film thicknesses, as measured by macroscopic KP, is shown. We find a decrease in the work function (ΔWF) of 0.2 eV for ITO/carbazole polymer electrodes when compared to untreated ITO. This shift did not show any significant variation with brush thickness over the range 12−40 nm suggesting that the brushes adopt an orthogonal orientation with respect to the surface, only in the vicinity of the substrate whereas in their upper parts the brushes lie progressively more flat, limiting the induced dipole for thicker layers.

Interestingly, on a scale of hundreds of nanometers, KPFM measurements revealed a larger negative shift of WF amounting ΔWF 0.68 $\pm$ 0.04 eV for carbazole polymer brushes grown on top of native silicon oxide substrate (*n*-doped, resistivity = 1−10 Ω/cm) with a thickness of ca. 30 nm. Such detected discrepancy with respect to the results by KP obtained from brushed on ITO can be due to differences in the growth of the brushes, e.g. induced by the ultraflat nature of the silicon substrate, which could result, for example, in a decreased density of brushes within the film. In addition, the increased substrate roughness in polymer films grown on ITO leads to more disorder assembly within the films. This leads to a smaller effective dipole contribution to the work function of the system.

To improve the order within the densely packed brushes and favor their packing, we used solvent vapor annealing (SVA) treatment.[36] Samples kept in a chloroform saturated atmosphere for 48 h exhibited a reduced work-function negative shift ΔWF = 0.58 $\pm$ 0.04 eV (as measure by KPFM). Given that the surface morphology upon SVA treatment appears unaltered, one can speculate that this change is due to a molecular reorganization within the film, leading to a less uniform orientation of the carbazole units, thus to a decrease in the effective dipole moment within the film.

3.5. Electroabsorption. To investigate this effect further, we incorporated the brushes into sandwich structure polymer light-emitting diodes (LEDs) and probed the internal fields by electroabsorption.[37] This technique uses an optical probe to measure internal fields in devices whose active layers show a Stark shift under an applied electric field. The device configuration we used is illustrated in the inset of the lower panel of Figure 5 and consists of an ITO anode with the carbazole functionalized polymer brushes grown on top, followed by a spin-coated layer (80 nm) of the much studied green light-emitting polymer poly(9,9′-dioctylfluorene-alt-benzothiadiazole) (F8BT), and an anode of calcium (50 nm) capped with a protective layer of aluminum (150 nm). The DC bias voltage is applied between the ITO anode and the Ca/Al cathode. By using monochromated light with 515 nm wavelength—on the low energy edge of the F8BT absorption band and away from the carbazole polymer absorption band—we were able to probe the internal fields of the F8BT layer only, allowing us to detect dipoles in the carbazole polymer brush layers.

Figure 6 shows the electroabsorption signal, $\Delta T/T$, plotted as a function of the DC bias applied across the device (swept from negative to positive bias). All curves have been normalized to $\Delta T/T = 1$ at $V_{dc} = -1.8$ V to aid visualization. The black line (representing the device with no brushes grown on the ITO) is typical of a device with an ITO electrode, showing a linear behavior and intercepting the *x*-axis at V_{DC} = 1.8 V. This intercept is the built-in voltage of the device, and assuming a work function for calcium of 2.8 eV,[38] it is in excellent agreement with our measurement of the work function of untreated ITO (4.6 eV).

The voltage scans for the devices incorporating the carbazole polymer brushes are not linear, which is a strong indication of a build-up of charge in the device. Given that the calcium cathode has a low work function with no barrier for electron injection into F8BT (the lowest unoccupied molecular orbital (LUMO) of F8BT is ~3.5 eV below vacuum), while there is simultaneously a large barrier for injection at the anode (the highest occupied molecular orbital of F8BT is ~5.9 eV),[39] the

(36) (a) De Luca, G.; Liscio, A.; Maccagnani, P.; Nolde, F.; Palermo, V.; Mullen, K.; Samori, P. *Adv. Funct. Mater.* **2007**, *17*(18), 3791–3798. (b) Treossi, E.; Liscio, A.; Feng, X.; Palermo, V.; Müllen, K.; Samor, P. *Small* **2009**, *5*(1), 112–119.

(37) (a) Latini, G.; Wykes, M.; Schlapak, R.; Howorka, S.; Cacialli, F. *Appl. Phys. Lett.* **2008**, *92*(1), 013511. (b) Winroth, G.; Latini, G.; Credgington, D.; Wong, L. Y.; Chua, L. L.; Ho, P. K. H.; Cacialli, F. *Appl. Phys. Lett.* **2008**, *92*(10), 103308. (c) Brown, T. M.; Kim, J. S.; Friend, R. H.; Cacialli, F.; Daik, R.; Feast, W. J. *Appl. Phys. Lett.* **1999**, *75*(12), 1679–1681.

(38) Park, Y.; Choong, V.; Ettedgui, E.; Gao, Y.; Hsieh, B. R.; Wehrmeister, T.; Mullen, K. *Appl. Phys. Lett.* **1996**, *69*(8), 1080–1082.

(39) Moons, E. *J. Phys.-Condens. Matter* **2002**, *14*(47), 12235–12260.

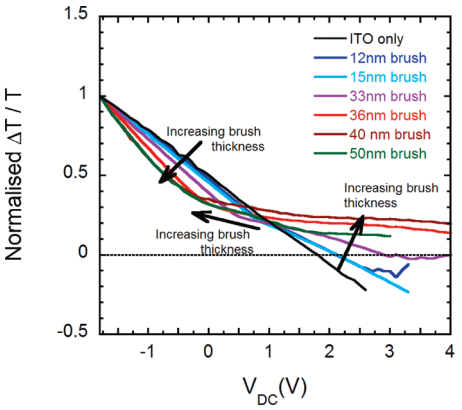

Figure 6. First harmonic electroabsorption signal vs applied bias across sandwich devices incorporating a carbazole based polymer brush layer. The structure of the devices is depicted in Figure 5 (lower panel inset). The data was obtained using a probe wavelength of 515 nm. To enable visual comparison, all curves are normalized to $\Delta T/T = 1$ at $V_{dc} = 1.8$ V.

charging is most likely due to electrons trapped in the device. This is also consistent with F8BT being a preferential electron transporter.[40] Alternatively or in addition, the observed deviation from linearity could also be due to a field-induced reorientation effect of dipoles in the brushes. The two effects could well be synergistic, in the sense that charge trapping might also assist the orientation of intrinsic brushes dipoles and their cooperative alignment. For thin brush layers, the charging/reorientation means that the $\Delta T/T = 0$ condition is reached at higher voltages than for ITO. For thicker brush layers (> 33 nm), this condition is never reached. We can still use the characteristics, however, to get an insight into the electric fields inside the devices in reverse bias or near the $V_{DC} = 0$ condition, by focusing on the sections of the voltage scans at low and negative voltages where there is no significant charge injection and it is thus possibly to get a linear fit to the data. Extrapolation of the linear fits can give us an estimate of the null voltage, V_{null}, where we would expect the condition $\Delta T/T = 0$ to be achieved in the absence of charging/reorientation. We take this to be a measure of the built-in voltage of the uncharged device.

We observe a huge dependence of V_{null} on brush thickness (Figure 5, lower panel, and Table 3), from 1.8 V for the ITO only device to just 0.14 V for the 50 nm brush device. This is consistent with the light turn-on voltages, V_{on}, observed for the same devices (Table 3), with V_{on} increasing from 3.2 V for ITO only devices to 14.1 V for devices incorporating 50 nm brush layers. This points to a decrease in work function of the ITO/brush electrode, as observed by Kelvin probe, except that in the device configuration we observe a dependence on brush thickness. This may be as a result of a more regular orientation of the brushes in the applied DC field or in the presence of charge of an applied bias, compared to the films used for the Kelvin probe characterization. The maximum luminance, L_{max}, from LEDs did not show

(40) Campbell, A. J.; Bradley, D. D. C.; Antoniadis, H. *Appl. Phys. Lett.* **2001**, *79*(14), 2133–2135.

Table 3. Properties of LEDs Incorporating a Carbazole Polymer Brush Layer and F8BT[a]

brush thickness (nm)	V_{null} (V)	V_{on} (V)	L_{max} (Cd/m^2)	η_{max} (%)
0 (ITO only)	1.76	3.2	29	0.0045
12	1.58	4.3	24	0.0040
15	1.57	4.0	48	0.0059
36	0.84	8.9	30	0.021
40	0.35	10.7	25	0.030
50	0.14	14.1	2.8	0.0099

[a] The device structure is illustrated in the inset of Figure 5. The external quantum efficiency, η_{max}, was measured at the maximum luminance, L_{max}.

a clear trend with brush thickness, and it should be noted that the devices with 50 nm brushes were destroyed by the high driving voltages before a high luminance was achieved. The higher external quantum efficiencies, η_{max}, for thicker brushes (Table 3) is consistent with the presence of a layer of trapped electrons in the device that enable a high recombination efficiency of holes.

4. Conclusion

Isocyanides exposing carbazole functionalities could be prepared by alanine coupling to a carbazole derivatized amine and subsequent conversion into an isocyanide. Upon polymerization of this monomer, the resulting polymer was insoluble in most common organic solvents; complete characterization was obtained by solid state spectroscopy. Homogeneous polymer brushes were grown on silicon wafers as well as on ITO anodes, giving a morphology of the brush layers indicative of aggregation of the chains at the molecular level. KPM of the surface dipoles revealed that the aggregates extend vertically away from the substrate. A small dipole is found; although for the thicker brushes, a less well-aligned layer is formed and hence a less pronounced effect. Incorporation of these brushes into LEDs was successful, and a large shift in the built-in voltage at zero bias was observed. However, with the effective work function of the anode being decreased, the devices showed much increased turn-on voltages. Current investigations are being carried out to resolve this problem. Both photovoltaic and FET devices based upon isocyanide brush materials have been made and will be published in a forth coming paper. The surface initiated polymerization of copolymers or block(co)polymers might open a way to improve the device characteristics.

Acknowledgment. Some of the authors gratefully acknowledge the financial support provided by EPSRC through the SONS II Programme of the European Science Foundation (SUPRAMATES project (O.F., F.C., A.L., V.P., P.S.) and the BIONICS project (V.P., P.S., A.E.R., R.J.M.N.). The Council for Chemical Sciences of The Netherlands Organization for Scientific Research (NWO−CW) (A.E.R.), the Royal Netherlands' Academy for Arts and Sciences (KNAW) (R.J.M.N.), the Technology Foundation STW (J.J.L.M., A.E.R.), the Netherlands Organization for Scientific Research NWO-TOP research grant, the EC FP7 ONE-P large-scale project no. 212311, the EC Marie Curie

ITN-SUPERIOR (PITN-GA-2009-238177), the NanoSciEra project SENSORS, and the Engineering and Physical Sciences Research Council (EPSRC, UK) (W.T.S.H.) are acknowledged for financial support.

Supporting Information Available: Figures S1−S10, Table S1 and tables of crystal data (S2−S7) for **5**, and an X-ray crystallographic file (CIF). This material is available free of charge via the Internet at http://pubs.acs.org.